9TH. INTERNATIONAL SYMPOSIUM ON FLOW VISUALIZATION, 2000

# FLOW DOWNSTREAM OF A BACKWARD FACING STEP ATTACHED TO A ROTATING CYLINDER

K. BREMHORST[+], J. BIENKOWSKI[+], S. NESIC[+] AND K.-S. YANG[#]

**Keywords: rotating cylinder, backward facing step, reattaching flow, turbulent transport enhancement, erosion-corrosion, direct numerical simulation**

## ABSTRACT

*Enhanced corrosion frequently occurs at surface disturbances introduced by fittings, valves, weld beads and other forms of geometric changes. Such flow enhanced corrosion is often mass transfer controlled due to increased species transport in the regions of disturbed flow. Towards a better understanding of such phenomena which are linked to electrochemical aspects of the fluid and surface interaction, a stepped rotating electrode has been developed consisting of two symmetrically placed backward facing steps on a rotating cylinder. Flow visualization studies using sulphuric acid vapour in air and surface dye dissolution, have been used together with surface heat and mass transfer measurements and DNS to help characterize the flow. While the classical reattachment behind a backward facing step is indicated by the results, DNS data have led to a new understanding of the reattaching flow and its highly unstable nature. The high turbulence generated by this flow is readily seen and differences between mean and fluctuating wall shear stresses are quantified. The observed flow patterns correlate with surface heat and mass transfer measurements. Findings suggest that the new stepped rotating electrode will be a convenient and useful tool for further flow related corrosion studies.*

## 1 INTRODUCTION

Single-phase flow affects metal loss, that is, corrosion in a number of ways, several of which are mass transfer related. Such processes are described by many overlapping terms, the most common being erosion-corrosion, which will be used in the present work. It is a well established fact that erosion-corrosion is more severe in the vicinity of flow disturbances which give rise to complex flow patterns with increased turbulence levels, mass transfer and surface stresses but the concept of "near wall turbulence" affecting corrosion still needs clarification and effective means of prediction [1].

Erosion-corrosion under disturbed flow conditions has been studied experimentally in flow loops [2] which are expensive, and numerically by performing flow simulations [3]. The advantages of rotating cylinder electrodes for such studies are well established [4]. In the present study the standard rotating cylindrical electrode, Fig. 1(a), is modified by addition of a step, Fig.1(b). This geometry promises to become an effective and cheap tool for studying erosion-corrosion under disturbed flow conditions once the fluid flow conditions have been fully characterized. Results of a pilot study involving dye visualization and wall heat and mass transfer measurements complemented with Direct Numerical Simulation (DNS) for visualization of the turbulent flow around the electrode are reported.

**Author(s):** + *Department of Mechanical Engineering, The University of Queensland*
# *Department of Mechanical Engineering, Inha University, 253 Yonghyum-Dong, Nam-ku, Inchon, 402-751, Republic of Korea*

*Corresponding author: Professor K. Bremhorst, Dept. of Mechanical Engineering, The University of Queensland, Brisbane, Qld. 4072, Australia, email:* bremhorst@mech.uq.edu.au
*Phone: +61 7 3365 3597, Fax: +61 7 3365 4799*

For a smooth cylinder, it is known that laminar flow occurs for cylinder Reynolds numbers, Re, below 200 [4,5], where Reynolds number is defined in terms of the surface peripheral velocity, $V$, the cylinder diameter and the fluid kinematic viscosity. In the case of the stepped cylinder, the inner cylinder diameter was used to define Reynolds number. Flow visualization and heat transfer studies were performed in air at room temperature while mass transfer measurements were performed with potassium ferri-/ferro-cyanide solution as the electrolyte. This was for experimental convenience and in the belief that similarity applies.

## 2 EXPERIMENTAL DETAILS

The stepped electrode, Fig. 1(b) consists of a solid inner cylinder over which is fitted a sleeve with a cutout to form the backward facing step. Two diametrically opposite steps are used in order to retain balance of the shaft. The sleeve can be rotated relative to the inner cylinder thus allowing the distance between a transducer fixed to the inner cylinder and the step to be varied. In the present case, the sleeve outer diameter was 24 mm, the inner cylinder diameter was 20 mm thus giving a step height, $h$, of 2 mm and the axial length of the cut out was 46 mm. The electrode was operated with a Pine Instruments rotator for accurate control of rotational speed.

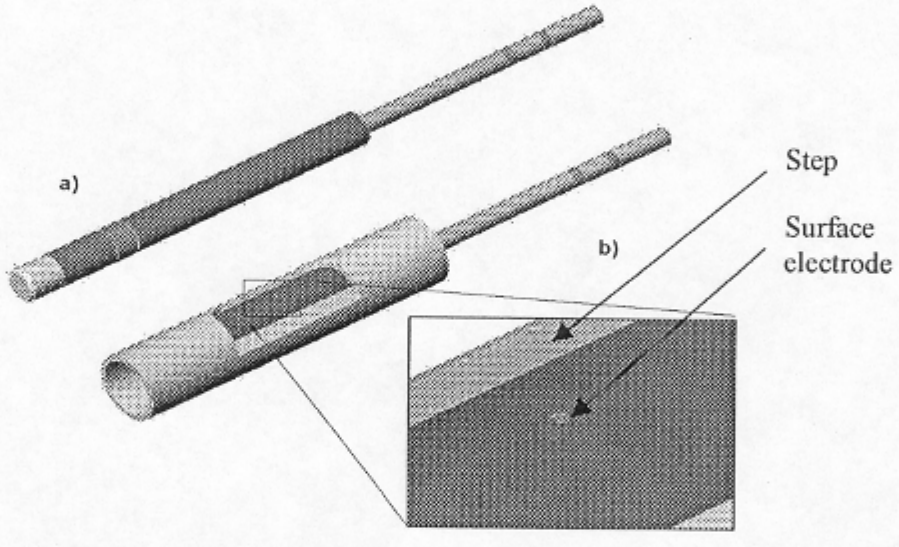


**Fig. 1. (a) A standard rotating cylinder electrode mounted on a shaft. (b) Rotating cylinder electrode with a step.**

## 3 RESULTS

### 3.1 Flow visualization

Flow visualization by use of sulphuric acid vapour injected from Dräger tubes close to the outer surface of the stepped cylinder operating in air gave clear views of the flow pattern at low rotational speeds. Images were captured with a video camera and subsequently digitized. These studies were limited to low rotational speeds when flow is still laminar. Once turbulence sets in, clarity is lost and the step area is no longer visible.

In Fig. 2(a), the flow (visualized by light circumferential streak lines) is seen to reattach very close to the rear face of the step, which is contrary to observations with turbulent flow over backward facing steps. As rotational speed is increased a transition phenomenon sets in where the

reattachment of Fig. 2(b) is observed but at other times the flow of Fig. 2(c) is observed where a radial burst is seen and is followed by reattachment behind the step. This burst due to centrifugal action is seen to increase in radial extent with increasing rotational speed, Fig. 2(d). At this stage the flow is laminar. At still higher rotational speeds, 140 revolutions per minute (rpm) and higher, the radial burst vanishes and is replaced by turbulence. The point of reattachment at this speed moved to some three step heights behind the step and the acid vapour technique ceased to be a useful flow visualization tool due to the turbulence and other flow disturbances.

In order to visualize higher speed turbulent flows, a line of dye was painted on the inner cylinder surface. Solvent was then injected parallel to the cylinder surface. As solvent touched the surface, the dye dissolved momentarily and was smeared in the direction of the instantaneous flow. By varying the distance from the step, *s*, to the dye, it was hoped to define the reattachment line behind the step. While an indication of reverse flow at one step height behind the step is clearly visible, Fig. 3(a), at three step heights behind the step reverse and forward flow are indicated to an equal extent, Fig. 3(b). DNS studies reported below indicate why a well defined separation of reverse and forward flow was not obtained. This method of flow visualization yielded good data between 1000 and 6500 rpm. Reversal of flow is clearly indicated in the region up to 2 step heights. Past this point, the dye streaks did not show clear bias in the forward or reverse direction.

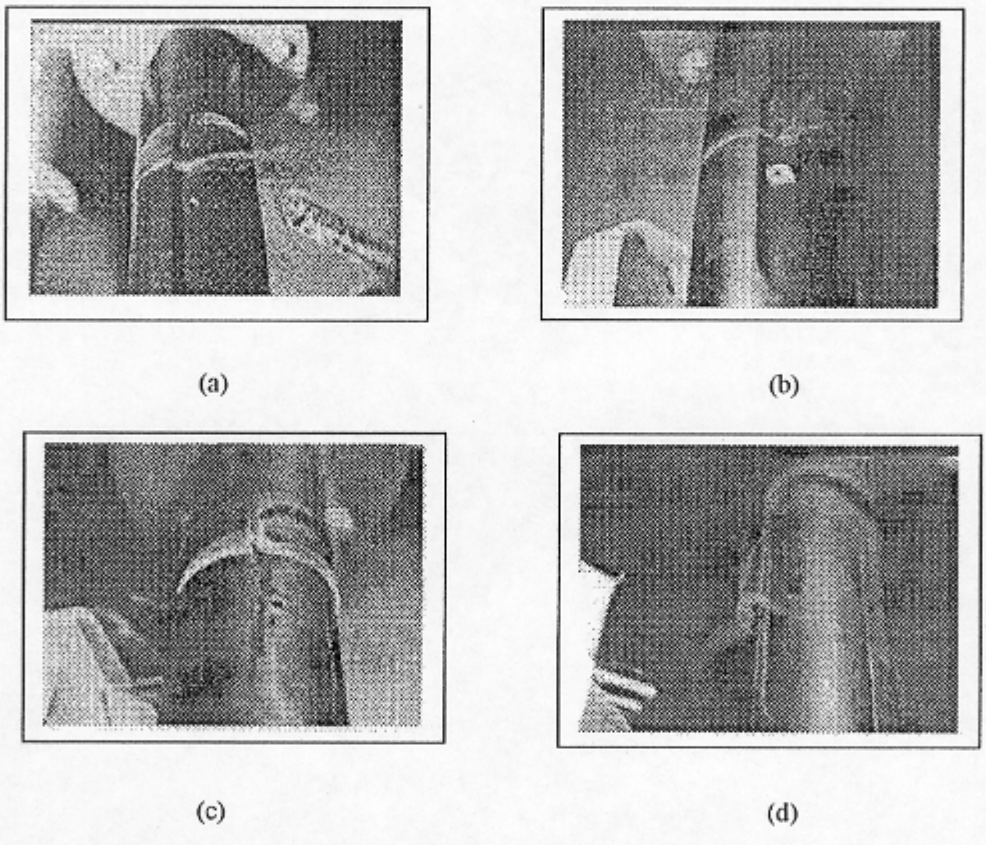


**Fig.2. Acid vapour flow visualization, (a) 10 rpm, Re = 13.7, V = 0.0105 m/s, (b) 100 rpm, Re = 137, V = 0.105 m/s, (c) 100 rpm, Re = 137, V = 0.105 m/s, (d) 140 rpm, Re = 191.8, V = 0.147 m/s.**

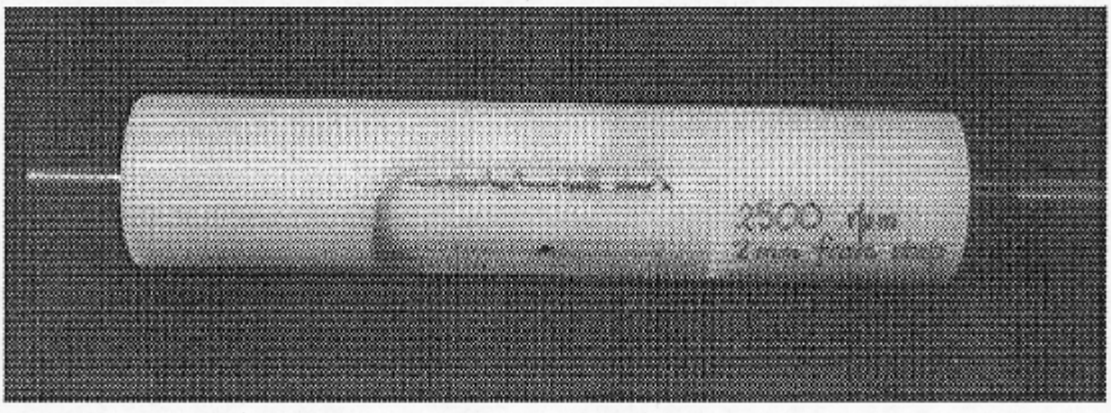


**Fig. 3(a). Dye flow visualization, 2500 rpm, Re = 3427, $V$ = 2.63 m/s $s/h$ = 1**

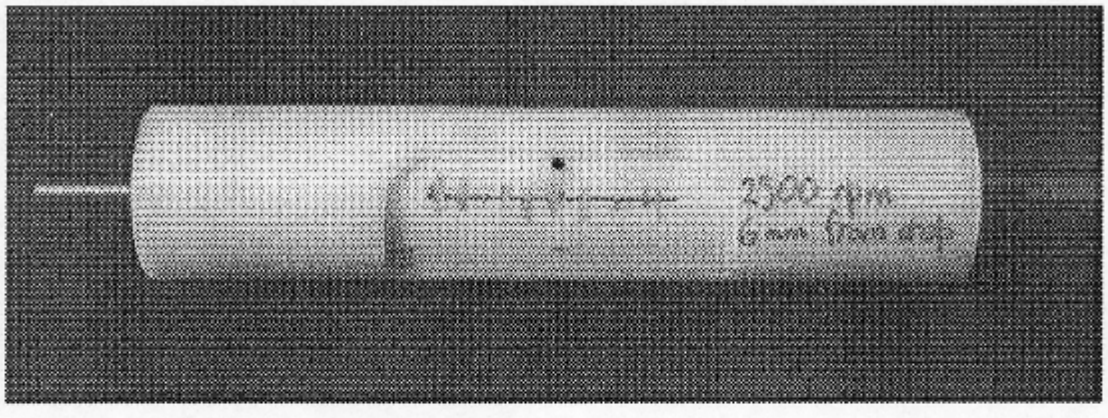


**Fig. 3(b). Dye flow visualization 2500 rpm, Re = 3427, $V$ = 2.63 m/s $s/h$ = 3**

### 3.2 Mass transfer enhancement

Mass transfer at the cylinder wall was measured by the limiting current technique with the potassium ferri-/ferro-cyanide reduction/oxidation reaction [6,7]. A 0.7 mm diameter platinum patch electrode mounted flush with the inner cylinder wall and a 80 mm ring electrode concentric with the cylinder electrode together with a reference electrode yielded the necessary electrochemical measurements. The choice of a patch electrode in place of a line or a full cylinder type was guided by the desire to ultimately investigate localized corrosion.

Data are reported as mass transfer enhancement ratios, Fig. 4. This is the ratio of mass transfer obtained behind the step relative to that without the step at the same rotational speed. It is seen that the expected variation of mass transfer for backward facing steps was obtained. The peak enhancement factor is 1.2 and is located near the reattachment line identified by visualization. Such increases in mass transfer can be obtained with a smooth cylinder by increasing the rotational speed by a factor of 1.34, which reflects the relationship between Sherwood number and Reynolds number. The major difference will be in the structure of turbulence associated with reattachment relative to that of a smooth cylinder. For a smooth cylinder the mean and fluctuating wall shear stresses increase with rotational speed while for the stepped cylinder mean shear stress vanishes at the reattachment point or line but fluctuating wall shear stress remains high. The consequence of this is not well understood in the context of erosion-corrosion and will be explored more fully in future work.

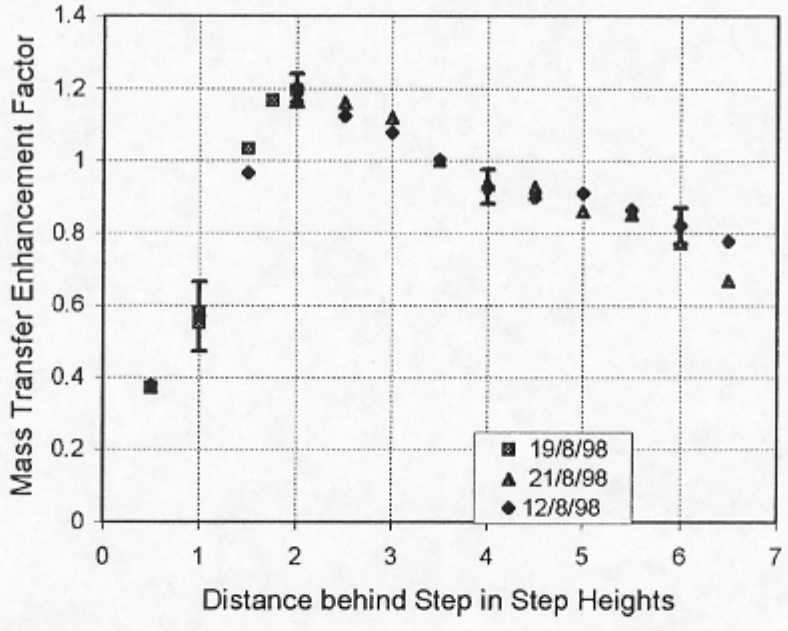


**Fig. 4. Enhancement of mass transfer behind the step as a function of distance behind the step for 500 rpm, Re = 9650, $V$ = 0.525 m/s. Error bars denote the 95% confidence limits and points taken on different days indicate the repeatability of the data points.**

It is noteworthy that immediately behind the step where recirculation of flow is expected, lower mass transfer rates are obtained than on a smooth cylinder. At 1.5 step heights behind the step, mass transfer is similar to that on a smooth cylinder and only further downstream is an enhancement of mass transfer obtained.

### 3.3 Heat transfer enhancement

Surface heat transfer measurements were obtained in air with a 1mm long platinum film mounted on the surface of the inner cylinder. The film gives a close approximation to the patch electrode used for mass transfer data of the previous section. Constant current heating was applied. Calibration of the film as a function of rotational speed was performed with the smooth cylinder, that is, with the outer sleeve removed. Consequently, measurements behind the step are relative to heat transfer obtained with the smooth cylinder, Fig. 5. The enhancement factor in this case is the smooth cylinder rotational speed giving the same heat transfer as that behind the step, relative to the rotational speed of the stepped cylinder.

Surface heat transfer distributions are seen to be similar to those observed for mass transfer, Fig. 4. The location of the peak is at almost the same distance behind the step. In the Reynolds number range of 1000 – 10000, the trend is for the position of the peak of mass and heat transfer measurements to decrease from 3.5 step heights to 2.5 as Reynolds number increases [8].

As for mass transfer, the region up to 1.25 step heights gives less heat transfer than the smooth cylinder. Further downstream, heat transfer is above that for the smooth cylinder and does not reduce below the smooth cylinder case as was the case for mass transfer. Differences between mass and heat transfer measurements could be due to the difference in the surface gauges (circular patch versus elongated hot-film element). Some of the difference could also be due to the working fluids as the Schmidt number of potassium ferri-/ferro-cyanide is 1224 whereas the Prandtl number of air is 0.71.

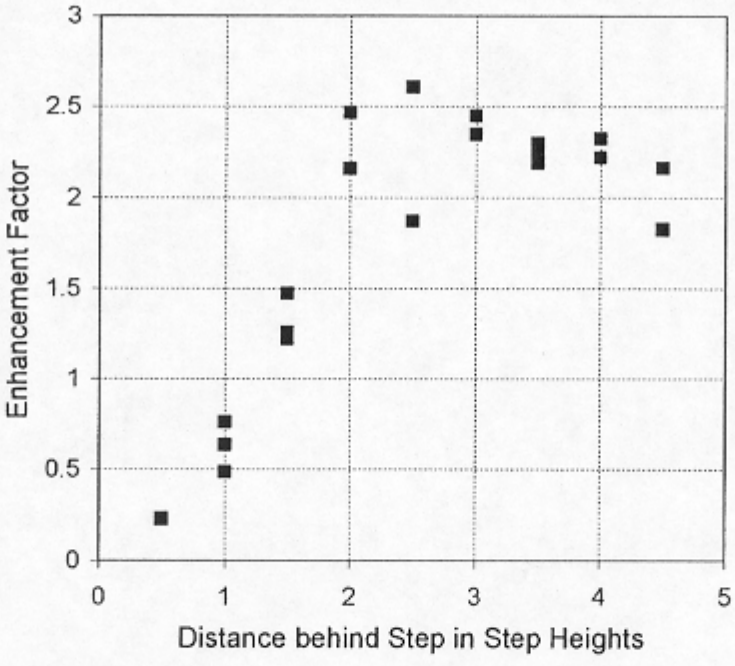


**Fig. 5. Enhancement of heat transfer behind the step at 7000 rpm, Re = 9569, V = 7.33 m/s.**

### 3.4 DNS visualization results

Reynolds numbers for the range of rotational speeds of interest are low enough to permit direct numerical simulation (DNS) of the Navier-Stokes equations in incompressible form. A reference frame rotating with constant angular velocity, $\Omega$, is used with the cylinder being held stationary. The governing continuity and momentum equations are (1) and (2) with the last term in Eq. (2) being the Coriolis acceleration. $u$, $\rho$ and $\nu$ denote the vector velocity relative to the rotating reference frame, density and kinematic viscosity respectively. Centrifugal acceleration does not appear explicitly as it has been included in the pressure term [9].

$$\nabla \cdot \mathbf{u} = 0 \tag{1}$$

$$\frac{\partial \mathbf{u}}{\partial t} + (\mathbf{u} \cdot \nabla)\mathbf{u} = -\frac{1}{\rho}\nabla P + \nu \nabla^2 \mathbf{u} - 2\Omega \times \mathbf{u} \tag{2}$$

These equations were discretized using a finite volume method. A fractional step method [10] was used to decouple the continuity and momentum equations. Nonlinear and cross-diffusion terms were advanced explicitly by a third-order Runge-Kutta scheme while the other terms were advanced by the Crank-Nicolson method. The geometric cross-section details are given in Fig. 6. It is assumed that the axial direction is infinite and homogeneous. Solutions were obtained for the hot-film experiments at Re = 2800, that is, for air as the working fluid. In order to limit the computational domain, the outer boundary representing the vessel containing the electrolyte and electrode was taken at 70 mm radius. The axial domain was limited to 24 mm. The computational grid was a body-fitted O-grid system with more resolution near the step and solid boundaries. The number of grid points was 224x128x80 (tangential, radial and axial) for the finest resolution computed. A typical run took 12,000 time steps, which corresponded to 10 revolutions of the cylinder.

A no-slip boundary condition was applied on the solid surfaces of the cylinder with a periodic boundary condition in both the tangential and axial directions. The outer boundary was represented

by the gradient conditions of Eq. (3), that is, a slip boundary condition was used in order to limit the spatial extent in the radial direction and in order to avoid the high resolution needed for a no-slip boundary condition at the vessel wall.

$$\frac{\partial u_\theta}{\partial n} = \Omega \qquad u_r = 0 \qquad \frac{\partial u_z}{\partial n} = 0 \tag{3}$$

where $u_\theta$, $u_r$ and $u_z$ represent the tangential, radial and axial velocity components respectively and $n$ is the outward normal direction at the surface. Flow averages were obtained over three revolutions of the cylinder after solutions had reached a statistically steady state. Averaging was performed along the cylinder as well as in time.

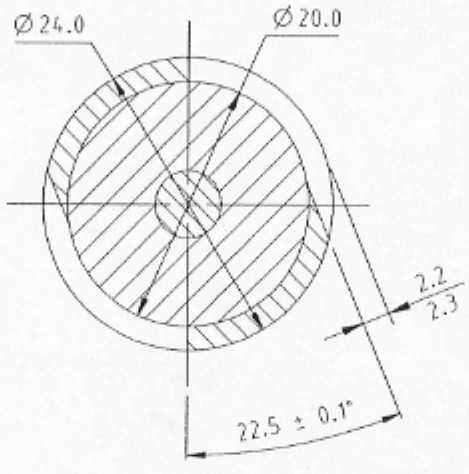


**Fig. 6. Cross-section of stepped electrode simulated by DNS, dimensions are in mm.**

The attached avi file gives a video sequence of the instantaneous flow. Two sequences are reproduced in Fig. 7, which give some indication of the extent of the fluctuating region of reverse flow at the surface. A consequence of this is that the instantaneous reattachment point varies over a large range of $s$, which is the distance along the surface from the base of the step. This is not reflected in the space/time averaged streamline plot of Fig. 8. The flow is seen to be an extensive region of highly fluctuating flow with a large but poorly delineated region of reverse flow. This helps to explain why clear lines separating forward and reverse flow were not easily observed with the dye flow visualization technique of Fig. 3 except immediately behind the cylinder. The video sequence also clearly shows that the corner flow at the base of the step is captured.

Furthermore, a feature not reflected by time averaged plots is that regions of reverse flow exist in the free flow. From a flow measurement point of view, this presents special problems as hot-wire anemometry generally does not detect flow reversals and laser Doppler anemometers can miss this aspect unless precautions are taken to ensure that adequate frequency shifting is employed.

The streamline plot, Fig. 8, indicates that a region exists which is similar to that behind backward facing steps found at sudden pipe expansions or other obstacles such as orifice plates. The downstream reattachment point is 4.9 step heights from the step, which contrasts strongly with the peak mass and heat transfer points located at approximately 3.5 step heights at low Reynolds numbers [8]. This is explored further in the next section. The reattachment length is significantly less than the $6.28h$ for a step in a plane geometry [11] although this could be due to the difference in Reynolds numbers. In the present case, the Reynolds number based on step height and peripheral velocity is 336 which compares with 5100 [11] also based on step height but free stream inlet velocity.

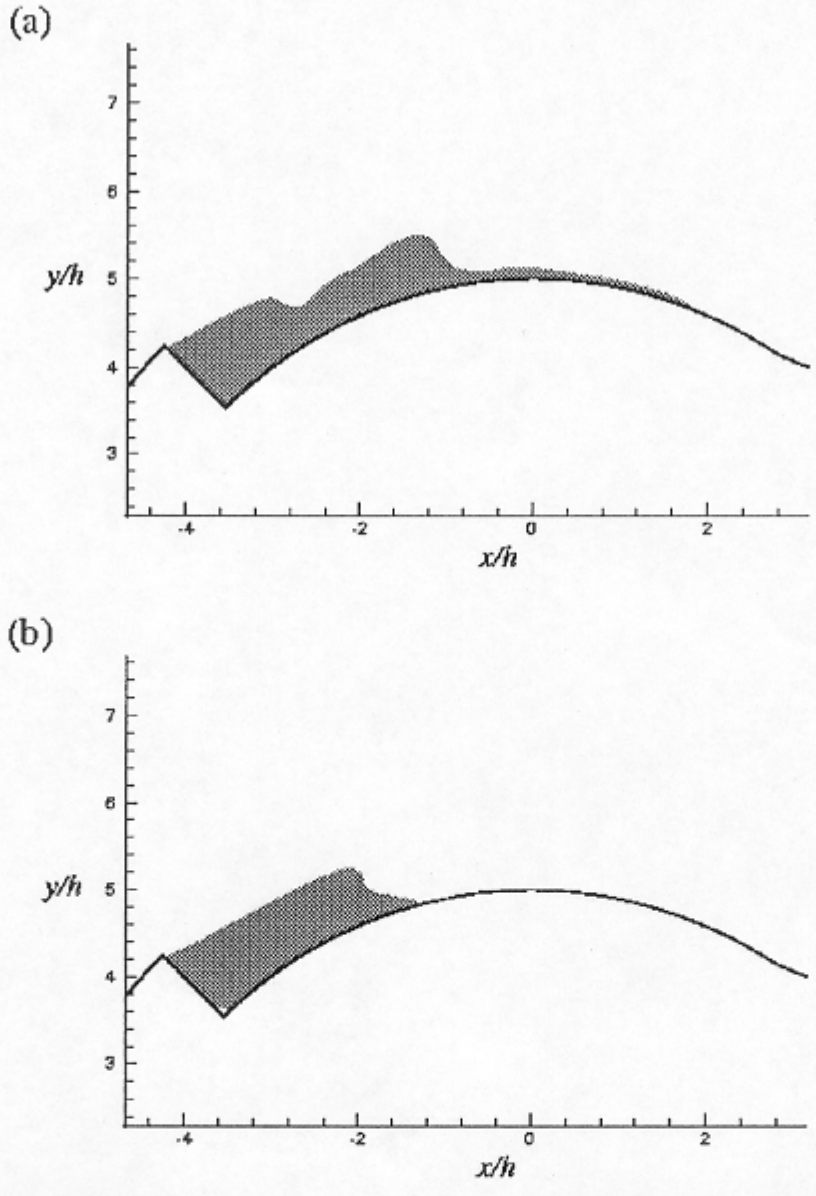


**Fig, 7. Instantaneous flow pattern (dark regions denote reverse flow) at the same axial cross-section and at two different times approximately 0.58 revolutions apart.**

### 3.5 DNS time averaged wall shear stress data

The DNS data have been averaged to yield mean and rms values of fluctuating velocity and wall shear stress, Fig. 9. Turbulence intensity is reported as $\sqrt{\frac{1}{3}\overline{u_i' u_i'}}$ where $u_i'$ denotes velocity fluctuation in each direction and Einstein summation is assumed for repeated indices. Values reported are taken at 0.006 step height from the wall and normalization is with $\frac{1}{2}\rho V^2$. Mean shear stress allows the reattachment point to be clearly identified at 4.9 step heights where mean shear stress vanishes. The peak of turbulence intensity occurs significantly upstream of the reattachment point. Turbulent shear stress also peaks well upstream of the reattachment point but almost coincides with the peak of negative wall shear stress although the value remains at a high level further downstream. Perhaps the most significant result is that the peak rms wall shear stress is above the mean shear stress, the peak of which occurs in the reverse flow region at about 3 step

heights rather than in the forward flow region downstream of reattachment. In terms of the heat and mass transfer results presented above, the peak in their distributions is just upstream of the peak shear stress distributions rather than near the reattachment point.

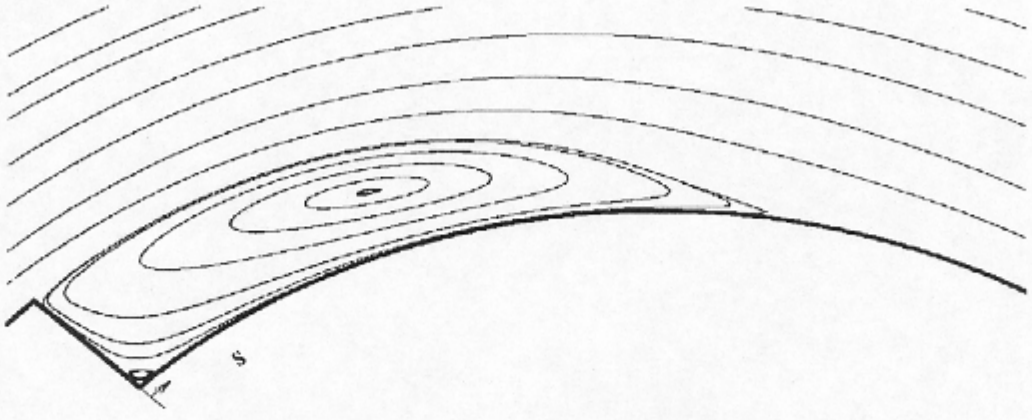


**Fig. 8. Predicted streamlines behind the step obtained by axial and time averaging.**

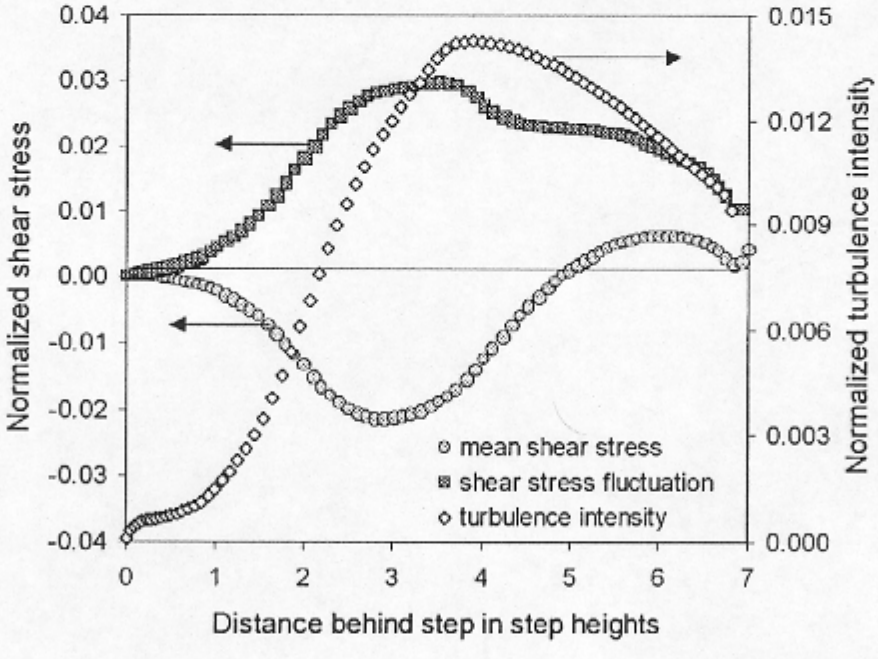


**Fig. 9. The normalized distributions of the mean tangential wall-shear stress, the rms of tangential wall-shear stress fluctuation, and the mean total turbulence intensity at 0.006 *h* away from the cylinder surface (all averaged in time and in the axial direction) as a function of distance behind the step.**

## 4 CONCLUSIONS

Traditional and DNS flow visualization studies of flow around a newly developed stepped rotating electrode indicate that a region of reattaching flow exists. Its general characteristics are similar to those of flow over a backward facing step. Visualization performed at low rotational speeds confirmed laminar flow for cylinder Reynolds numbers below 200. At the lowest speeds, flow reattachment occurs immediately behind the step. As rotational speed increases, centrifugal effects appear but DNS studies at higher rotational speeds in the turbulent flow regime show no visible effect due to centrifugal effects. A novel dye dissolution technique shows that a region of flow recirculation exists for at least 2 step heights downstream of the step, which is consistent with DNS results.

Surface heat and mass transfer measurements show a clear peak at 2.5-3.5 step heights behind the step, the position of the peak moving towards the step with increasing Reynolds number. A significant difference exists between heat and mass transfer results downstream of the peak although the positions of the peaks correspond closely.

DNS data indicate a higher level of fluctuating wall shear stress than mean shear stress and that the highest mean shear stress is within the recirculation region. The position of these peaks corresponds more closely with those of heat and mass transfer, which may have significant implications for erosion-corrosion effects in reattaching flows to be the subject of future studies.

## ACKNOWLEDGMENTS

The experimental study reported here was supported in part by an Australian Research Council grant. Their help is greatly appreciated. The computational part of the research was financially supported by 1998 CRAY R&D Research Fund in Korea and by a grant from The University of Queensland. Computations in the present work were carried out by using the CRAY C90 of the KORDIC supercomputer center in Korea, which is gratefully acknowledged.

## REFERENCES

[1] Nesic, S. and Postlethwaite, J.: Hydrodynamics of disturbed flow and erosion-corrosion, Part I, Single-Phase Flow Study. Canadian Journal Chemical Engineering, 69, p. 698, 1991.

[2] Lotz U. and Postlethwaite, J.: Erosion-corrosion in disturbed two-phase liquid/particle flow. Corrosion Science, 30, p. 95, 1990.

[3] Nesic, S. and Postlethwaite, J.: Relationship between the structure of disturbed flow and erosion-corrosion. Corrosion Journal, 46, p. 874, 1990.

[4] Gabe, D.R. Wilcox, G.D., Gonzalez-Garcia, J. and Walsh, F.C.: The rotating cylinder electrode: its continued development and application. Journal of Applied Electrochemistry, 28, pp 759-780, 1998.

[5] Nesic, S., Solvi, G.T. and Enerhaug, J.: Comparison of the rotating cylinder and pipe flow tests for flow sensitive carbon dioxide corrosion. Corrosion, 51, 10, pp 773-787, 1995.

[6] Efird, K.D.: Effect of fluid dynamics on the corrosion of copper-base alloys in sea water. Corrosion Journal, 33, p. 3, 1977.

[7] Newman, J.S.: Electrochemical Systems, Second Edition. Prentice Hall, Englewood Cliffs, New Jersey, 1991

[8] Bienkowski, J.: A rotating cylinder electrode with surface roughness. Honours Thesis, Department of Mechanical Engineering, The University of Queensland, Brisbane, Australia.

[9] Lezius, D.K. and Johnston, J.P.: Roll-cell instabilities in rotating laminar and turbulent channel flows. Journal of Fluid Mechanics, 77, p. 153, 1976.

[10] Rosenfeld, M. Kwak, D. and Vinokur, A.: Fractional step solution method for unsteady incompressible Navier-Stokes equations in generalized coordinate systems. Journal of Computational Physics, 94, p. 102, 1994.

[11] Hung Le, Moin, P. and Kim, J.: Direct numerical simulation of turbulent flow over a backward-facing step. Journal of Fluid Mechanics, 330, pp349-374, 1997.